

# Single-File Diffusion of Active Brownian Particles

Akinlade Akintunde,<sup>1</sup> Parvin Bayati,<sup>1</sup> Hyeongjoo Row,<sup>2</sup> and Stewart A. Mallory<sup>1,3,\*</sup>

<sup>1</sup>*Department of Chemistry, The Pennsylvania State University, University Park, Pennsylvania, 16802, USA*

<sup>2</sup>*Department of Chemical and Biomolecular Engineering, UC Berkeley, Berkeley, CA 94720, USA*

<sup>3</sup>*Department of Chemical Engineering, The Pennsylvania State University, University Park, Pennsylvania, 16802, USA*

(Dated: November 15, 2024)

Single-file diffusion (SFD) is a key mechanism underlying transport phenomena in confined physical and biological systems. In a typical SFD process, microscopic particles are restricted to moving in a narrow channel where they cannot pass one another, resulting in constrained motion and anomalous diffusion at long times. In this study, we use Brownian dynamics simulations and analytical theory to investigate the SFD of active Brownian particles (ABPs) – a minimal model of active colloids. Using a combination of scaling relations and heuristic arguments, we derive an accurate analytical expression for a tagged ABP's mean square displacement (MSD). We find the MSD exhibits ballistic behavior at short times, which can quantitatively be related to the reduced kinetic temperature of the single-file ABP system. We also find that while the characteristic subdiffusive scaling of SFD [ $\langle(\Delta x)^2\rangle \sim t^{1/2}$ ] is preserved at long times, self-propulsion introduces significant modifications to the 1D-mobility, which can be directly related to the constant Péclet (Pe) compressibility. Furthermore, we demonstrate that the generalized 1D-mobility, initially proposed by Kollmann for equilibrium systems [Phys. Rev. Lett. **90**, 180602 (2003)], can be extended to active systems with minimal modification. These findings have important implications for tuning particle transport at the microscale and provide a basis for understanding active matter in geometries with highly restricted motion.

## INTRODUCTION

For over half a century, single-file diffusion (SFD) has captivated researchers across the physical and biological sciences, finding broad applications in quantifying transport at the microscale [1–19]. In a typical SFD process, microscopic particles are confined to move within a narrow channel where they cannot pass one another (See Fig. 1 for a schematic illustration of SFD). This form of confinement leads to subdiffusive behavior at long times, making SFD one of the simplest examples of anomalous diffusion [20–27]. As a result, SFD provides a fundamental framework for understanding transport in highly confined systems, with far-reaching implications for both theoretical studies and practical applications.

Most studies of SFD have focused on equilibrium Brownian particles (i.e., passive particles), where it is nearly universally observed that, at long times, the mean square displacement (MSD) of a tagged particle scales as

$$\lim_{t \rightarrow \infty} \langle(\Delta x)^2\rangle = 2Ft^{1/2}, \quad (1)$$

where  $F$  is a proportionality constant known as the 1D-mobility. This characteristic subdiffusive scaling of SFD has been thoroughly explored computationally and experimentally in various systems, including colloidal particles in microchannels [28–33] and molecular transport in zeolites and carbon nanotubes [34–37]. In addition to experimental studies, several theoretical approaches have been developed to describe the SFD of passive Brownian systems, including fluctuating hydrodynamics [38–40], fractional Langevin formalisms [41–43], and asymptotic methods [44–46]. We refer the reader to Refs [25, 47–49], for a more comprehensive discussion on passive SFD.

The central theoretical challenge in SFD is to capture the many-body effects that give rise to subdiffusive behavior at long times and to quantitatively predict the 1D mobility. In one of the earliest studies of SFD, Harris [20] derived the fundamental result for the 1D-mobility of passive hard particles

$$F_{HR} = \frac{1 - \phi}{\rho} \sqrt{\frac{D}{\pi}} = \lambda \sqrt{\frac{D}{\pi}}, \quad (2)$$

where  $D$  is the free diffusion coefficient of the particle,  $\phi = \rho\sigma_p$  is the packing fraction,  $\sigma_p$  is the particle diameter, and  $\rho$  is the particle line density. The mean free path  $\lambda$ , which represents the average distance a particle can move before encountering its neighbor, can be calculated analytically for single-file passive hard particles and is given by  $\lambda = (1 - \phi)/\rho$  [50]. In Harris's derivation of the 1D-mobility, the mean free path is a fundamental quantity that provides a measure of the confinement experienced by a tagged particle and can be introduced to further simplify Eq. (2). We also find the mean free path plays a similar pivotal role in the SFD of active colloids.

More recently, using an asymptotic approach, Kollmann generalized the 1D-mobility for passive particles to systems with arbitrary finite-range interactions [10]. In such systems, the 1D-mobility is expressed as

$$F = \frac{1}{\rho} \sqrt{\frac{D\mathcal{X}}{\pi}}, \quad (3)$$

where  $\mathcal{X}$  is the reduced isothermal compressibility, defined as the ratio between the compressibility of an interacting system to that of an ideal system. We should note that for more complicated interparticle interactions,

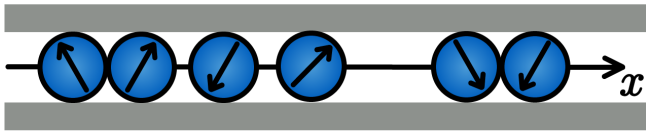


FIG. 1. Schematic of SF-ABP system. Each purely repulsive active particle moves at a constant speed of  $U_a \cos \theta$  while undergoing rotational Brownian motion with a reorientation time of  $\tau_R$ .

the quantity  $\sqrt{\mathcal{X}}/\rho$  plays a similar role to the mean free path introduced in Eq. (2). This generalized result has been verified across various systems, including attractive particles, mixtures, and particles with long-ranged interactions [29, 32, 51]. Interestingly, the work of Kollmann and others illustrates a peculiar feature of single-file systems: the 1D-mobility, a single-particle transport property, can be related to a thermodynamic response function of the system (i.e., the isothermal compressibility).

Much of the prior work on SFD has focused on passive particles, motivating the natural question: how is single-file diffusion altered when particle dynamics deviate from passive Brownian motion? To answer this question, we focus on active colloids capable of self-propulsion at the microscale. Interestingly, this novel class of colloids exhibits persistent directed motion at short times and undergoes diffusive motion at long times. The self-driven nature of active colloids has spurred extensive investigations into their phenomenology and use in potential applications ranging from transport, self-assembly, and fluid mixing at the microscale [52–67]. This includes several studies that have explored different aspects of single-file active matter systems [68–76]. However, there has been no systematic attempt to quantify the role of activity in single-file systems and how it influences observables such as the 1D-mobility. Understanding the SFD of active colloids is critical, as many proposed applications operate in environments where such conditions are likely.

In this work, we investigate the single-file diffusion (SFD) of active colloids within the context of the active Brownian particle (ABP) model. Here, we analyze the long- and short-time behavior of the mean square displacement (MSD), focusing on how self-propulsion modifies both the ballistic motion at short times and the sub-diffusive scaling at long times. Our results demonstrate that Kollmann’s generalized 1D-mobility expression for passive systems [Eq. (3)] can be extended to active systems with minimal modification. This work provides new insights into the behavior of confined active matter informing the design of microfluidic systems and targeted transport technologies, where precise control of particle dynamics is essential.

## Model

In this study, we consider a periodic single-file active Brownian particle (SF-ABP) model [77], where  $N$  purely-repulsive active Brownian disks are confined to move along a narrow channel of length  $L$ , as depicted in Fig. 1. The channel is sufficiently narrow to prevent particles from passing one another, enforcing a single-file condition that restricts their motion to one spatial dimension. Each particle experiences a self-propelling force  $F_a = \gamma U_a \cos \theta$ , where  $\theta$  is the angle between the particle’s orientation vector and the positive x-axis,  $\gamma$  is the translational drag coefficient, and  $U_a$  is the constant self-propelling speed. The orientation of each particle undergoes rotational Brownian motion with a characteristic reorientation time  $\tau_R$ . The following overdamped equations describe the motion of a tagged particle:

$$v = \dot{x} = U_a \cos(\theta) + \gamma^{-1} F_c, \quad (4a)$$

$$\dot{\theta} = \xi(t), \quad (4b)$$

where  $F_c$  represents the interparticle forces, and  $\xi(t)$  is the stochastic rotational noise with properties  $\langle \xi(t) \rangle = 0$  and  $\langle \xi(t)\xi(t') \rangle = (2/\tau_R)\delta(t-t')$ . For simplicity, we assume translational Brownian motion and hydrodynamic interactions are negligible. The interparticle forces  $F_c$  are implemented using a Weeks-Chandler-Anderson (WCA) potential, characterized by a potential strength  $\varepsilon$  and Lennard-Jones diameter  $\sigma$  [78]. We choose the potential strength to be sufficiently large (i.e.,  $\varepsilon/(F_a\sigma) = 100$ ) to effectively mimic hard-particle behavior endowing particles with an effective hard diameter of  $\sigma_p = 2^{1/6}\sigma$ . For the initial configuration, particles are randomly placed in the channel without overlaps, and the initial angles for the orientation vectors are uniformly distributed. Simulations were performed using HOOMD-blue [79] with  $N = 1000$  particles for a minimum of  $1.5 \times 10^{10}$  timesteps, and a timestep size  $\delta t = 10^{-5}$  time units.

The state of the SF-ABP system is characterized by two dimensionless parameters: the packing fraction  $\phi = \rho\sigma_p$ , where  $\rho = N/L$  is the particle line density, and the active Péclet number  $Pe = \ell_0/\sigma$ , where  $\ell_0 = U_a\tau_R$  is the intrinsic run length of a particle. The active Péclet number quantifies the persistence of a particle’s motion relative to its diameter. In the limit  $Pe \rightarrow 0$ , particles undergo nearly Brownian dynamics and we recover the mechanical, structural, and transport properties of the single-file hard particle system often referred to as the Tonks gas [80]. As  $Pe$  increases, large dynamic clusters begin to form [74, 81, 82]. A detailed analysis of clustering behavior in the SF-ABP system is provided in Ref. [74, 77, 83, 84]. Interestingly, despite significant clustering, the SF-ABP system does not exhibit a motility-induced phase transition at finite Péclet numbers [74, 81, 85, 86].

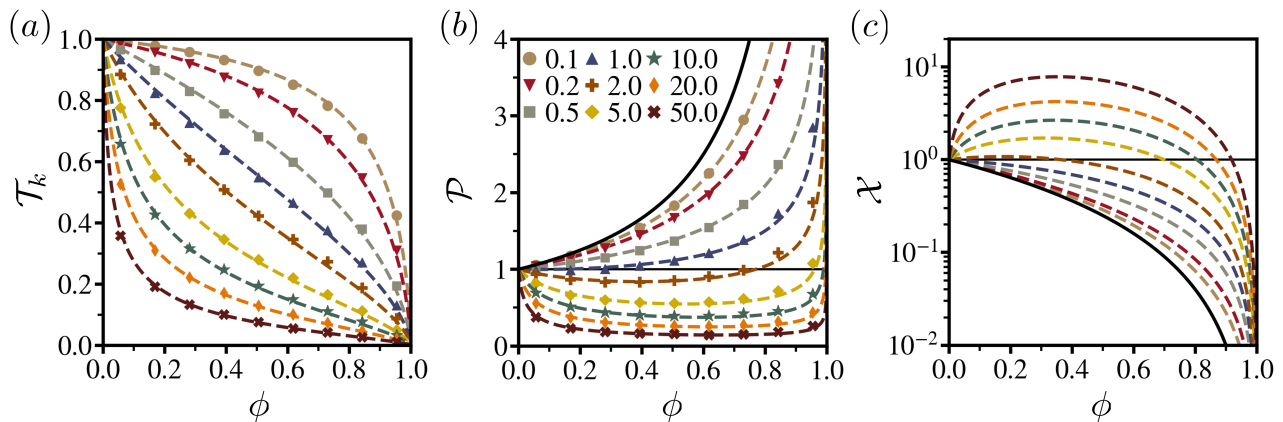


FIG. 2. Brownian dynamics simulation results (points) for the reduced (a) kinetic temperature, (b) pressure, and (c) constant Pe compressibility for different active Péclet numbers. The dashed colored lines in (a)-(c) correspond to the analytical expressions for these various quantities [Eqs. (6)-(8)]. While, the solid line in panels (b) and (c) corresponds to the analytical expression for the reduced pressure and isothermal compressibility for the 1D passive hard particle system (Tonks gas), respectively.

Here, we briefly summarize the concepts of kinetic temperature, pressure, and compressibility for the SF-ABP system, which are essential quantities for characterizing the MSD of a tagged particle [77]. The reduced kinetic temperature  $\mathcal{T}_k = 2\langle v^2 \rangle / U_a^2$ , which represents the ratio of the mean square velocity in the interacting system to that of an ideal SF-ABP system, is expressed as:

$$\mathcal{T}_k = 1 - \frac{2\langle F_c^2 \rangle}{(\gamma U_a)^2}, \quad (5)$$

where  $\mathcal{T}_k$  quantifies the reduction in the mean square velocity due to interparticle collisions. In Fig. 2(a), we show simulation results (points) for the reduced kinetic temperature of the SF-ABP system. As  $\phi \rightarrow 0$ ,  $\mathcal{T}_k \rightarrow 1$ , and as  $\phi \rightarrow 1$ ,  $\mathcal{T}_k \rightarrow 0$ . Using scaling arguments based on collision timescales, we previously derived the following accurate expression for the reduced kinetic temperature [dashed lines in Fig. 2(a)]:

$$\mathcal{T}_k = \frac{1}{9b^2} \left[ 2 \cos \left( \frac{1}{3} \arccos \left( \frac{27}{2} b^2 - 1 \right) \right) - 1 \right]^2, \quad (6)$$

where  $b = \alpha \text{Pe} \phi / (1 - \phi)$  and  $\alpha = c / (1 + \text{Pe})^d$  with  $c = 1.1$  and  $d = 0.05$ . Furthermore, we demonstrated that the reduced kinetic temperature is equivalent to the reduced swim pressure,  $\mathcal{T}_k = P_s / P_0$ , and derived an analytical expression for the reduced total pressure of the SF-ABP system:

$$\mathcal{P} = \frac{P}{P_0} = \mathcal{T}_k \left[ \frac{1}{1 - \phi} \right], \quad (7)$$

where  $P_0 = \rho \gamma U_a^2 / 2$  is the ideal gas pressure. In the limit of small Pe,  $\mathcal{T}_k \rightarrow 1$  and Eq. (7) reduces to the well-known equilibrium result for the Tonks gas  $\mathcal{P} = 1 / (1 - \phi)$  [80]. Fig. 2(b) shows a comparison between the reduced pressure for the SF-ABP system and Eq. (7).

The reduced constant Péclet compressibility,  $\mathcal{X}$ , [plotted in Fig. 2(c)] serves as a thermodynamic-like response function, analogous to the reduced isothermal compressibility in passive systems [77, 87]. This response function measures clustering and local density fluctuations, and as we show, is an important quantity in characterizing the MSD of a tagged particle. It can be calculated directly from Eq. (7), yielding

$$\mathcal{X} = \frac{\chi_a}{\chi_0} = \left[ \frac{\mathcal{T}_k}{(1 - \phi)^2} + \frac{\phi}{1 - \phi} \left( \frac{\partial \mathcal{T}_k}{\partial \phi} \right) \right]^{-1}, \quad (8)$$

where  $\chi_a = (\partial \ln \rho / \partial P)_{\text{Pe}}$  and  $\chi_0 = 1 / P_0$  are the compressibilities of the interacting and ideal systems, respectively. As  $\text{Pe} \rightarrow 0$ , the SF-ABP system recovers the passive result,  $\mathcal{X} = (1 - \phi)^2$ , and as  $\phi \rightarrow 0$ ,  $\mathcal{X} \rightarrow 1$ .

Before presenting the results of this study, we briefly review the mean square displacement (MSD) of an ideal suspension of SF-ABPs. A useful form of the MSD is

$$\langle (\Delta x)^2 \rangle = 2\langle v^2 \rangle t \left[ \int_0^t \left( 1 - \frac{\tau}{t} \right) \mathcal{V}(\tau) d\tau \right], \quad (9)$$

where  $\mathcal{V}(\tau) = \langle v(0)v(\tau) \rangle / \langle v^2 \rangle$  is the normalized velocity autocorrelation function and  $\langle v^2 \rangle$  is the mean square velocity of the particle [88]. In the ideal SF-ABP system, where there are no interparticle forces ( $F_c = 0$ ), it is straightforward to show that  $\langle v^2 \rangle = \frac{1}{2} U_a^2$  and  $\mathcal{V}(\tau) = e^{-\tau / \tau_R}$ . Substituting these two expressions into Eq. (9), we obtain the well-known result for ideal ABPs [89]:

$$\langle (\Delta x)^2 \rangle = 2D_0 \left[ t + \tau_R \left( e^{-t / \tau_R} - 1 \right) \right], \quad (10)$$

where  $D_0 = \frac{1}{2} U_a^2 \tau_R$  is the free diffusion coefficient of an ABP. The MSD of an ideal ABP exhibits two distinct scaling regimes. At short times, the motion is ballistic,

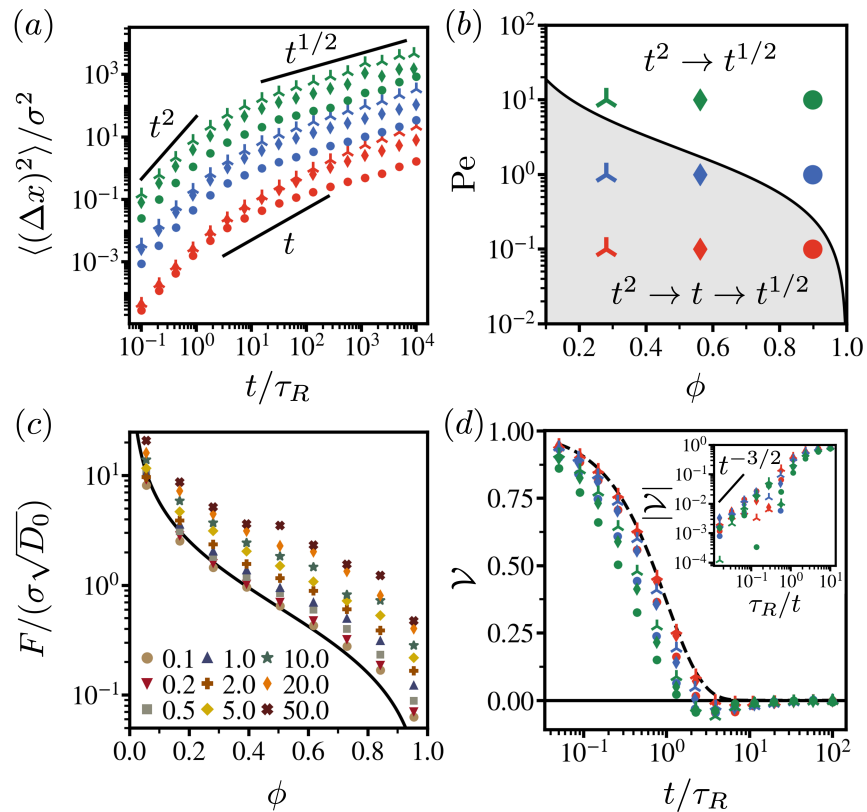


FIG. 3. (a) Mean square displacement (MSD) of a tagged particle in the SF-ABP system. (b) The state diagram for the SF-ABP system, with data points corresponding to the MSD curves in (a). The black line represents the condition  $\ell_0/\lambda_{ABP} = 1$ , separating two different dynamical regimes as discussed in the text. (c) Simulation results for the 1D-mobility across different values of  $Pe$  and  $\phi$ . The solid black line represents the analytical result for the 1D-mobility of passive hard particles [Eq. (2)]. (d) Normalized velocity autocorrelation function for the representative values of  $Pe$  and  $\phi$ . The solid black line represents the analytical result for ideal ABPs. The inset shows the power-law decay of the normalized velocity autocorrelation function, demonstrating the characteristic  $-t^{-3/2}$  behavior.

scaling as  $\langle(\Delta x)^2\rangle \sim \frac{1}{2}U_a^2 t^2$ . At long times, the motion becomes diffusive, scaling as  $\langle(\Delta x)^2\rangle \sim 2D_0 t$ . The crossover between the ballistic and diffusive regimes occurs around  $t \approx \tau_R$ , corresponding to the timescale over which the particle's orientation undergoes significant reorientation due to rotational diffusion.

## RESULTS

Figure 3 summarizes the simulation results for the SF-ABP system. The mean square displacement (MSD) for a representative selection of packing fractions and Péclet numbers is shown in Fig. 3(a). For all values of  $Pe$  and  $\phi$ , the MSD exhibits ballistic behavior at times less than the reorientation time  $\tau_R$ . At sufficiently long times, for all values of  $Pe$  and  $\phi$ , the MSD transitions to the characteristic subdiffusive scaling of single-file diffusion, where  $\langle x^2(t)\rangle \sim t^{1/2}$ . For a few cases, at low volume fractions, the crossover to the characteristic subdiffusive scaling regime occurs outside the time range shown in

Fig. 3(a), which we have cropped for visibility. However, we confirmed via simulation all values of  $Pe$  and  $\phi$  exhibit subdiffusive scaling at sufficiently long times. A general trend observed in Fig. 3(a) is that the overall magnitude of the MSD increases with  $Pe$ , and decreases with  $\phi$ . In addition, the crossover between the different scaling regimes exhibits a nontrivial dependence on  $Pe$  and  $\phi$ , which we discuss in the next section.

A more detailed analysis of Fig. 3(a) reveals two distinct scenarios in the MSD's behavior. In some cases, the MSD transitions directly from a ballistic regime to a subdiffusive regime. However, for certain values of  $Pe$  and  $\phi$ , a regime with diffusive character emerges at intermediate times (i.e.,  $\langle x^2(t)\rangle \sim t^\alpha$  where  $\frac{1}{2} < \alpha < 2$ ). This diffusive regime is typically observed when  $Pe$  or  $\phi$  are small, and collisions with neighboring particles are infrequent. Figure 3(b) provides a state diagram for the SF-ABP system and a simple scaling argument that approximately delineates these two MSD scenarios. The solid line in Fig. 3(b) corresponds to the condition where



the particle run length  $\ell_0$  equals the mean free path  $\lambda$ . For values of  $Pe$  and  $\phi$  above this line, the MSD transitions directly from ballistic to subdiffusive behavior. Below this line, an intermediate diffusive regime is observed. Here, we estimate the mean free path as the average distance between the edges of adjacent clusters. In prior work, we showed the mean free path is well-approximated by  $\lambda_{ABP} = (1 - \phi)/(\rho\mathcal{T}_k^\beta) = \lambda/\mathcal{T}_k^\beta$ , where  $\beta \approx 0.75$  and  $\lambda$  is the mean free path of the passive SF system [77]. Subdiffusive behavior in single-file systems is largely attributed to caging effects caused by collisions with neighboring particles [90, 91]. When  $\ell_0/\lambda_{ABP} > 1$ , particles move ballistically between collisions with their neighbors, preventing any diffusive behavior in the MSD. In contrast, when  $\ell_0/\lambda_{ABP} < 1$ , particles exhibit more diffusive motion between collisions. A similar result has been observed in studies of passive single-file particles, where the onset of subdiffusive behavior typically arises when  $t \approx \lambda^2/D$  [92–94]. In a later section, we calculate the local exponent of the MSD, which provides a more quantitative picture of the crossover dependence of the various scaling regimes.

In Fig. 3(c), we show the 1D-mobility  $F$  measured from simulation, alongside the analytical result for the 1D-mobility of the passive hard particle system [Eq. (2)]. As expected, in the limit  $Pe \rightarrow 0$ , the 1D-mobility converges to the analytical result for the passive system. For all values of  $Pe$ , the 1D-mobility decreases monotonically with increasing packing fraction. At higher packing fractions, particles experience more frequent collisions with neighboring particles, reducing mobility as crowding effects intensify. In contrast, for fixed  $\phi$ , the 1D-mobility increases with increasing  $Pe$ , reflecting the impact of self-propulsion on particle dynamics. As  $Pe$  increases, particles move more persistently, allowing them to overcome some of the crowding effects imposed by neighboring particles, thus increasing their effective mobility.

In Fig. 3(d), the normalized velocity autocorrelation function is shown for the representative selection of  $Pe$  and  $\phi$ . Across all values of  $Pe$  and  $\phi$ , the autocorrelation function exhibits self-similar behavior, characterized by an initial exponential decay, followed by a negative minimum between  $\tau_R < t < 10\tau_R$ , and a subsequent power-law decay back to zero. The relaxation time of the normalized velocity autocorrelation function, relative to the ideal case, decreases with increasing  $Pe$  and  $\phi$ , indicating faster decorrelation of particle velocities in systems with higher activity or packing fraction. The normalized velocity autocorrelation for the ideal case is plotted in Fig. 3(d) for reference (dashed black line).

The power-law decay of the velocity autocorrelation function, which has characteristic scaling  $-t^{-3/2}$  [see inset of Fig. 3(d)], has been widely observed in earlier simulations and experiments of passive systems [95]. In passive single-file systems, this decay arises from long-lasting correlations imposed by caging effects. This power-law

behavior, or long-time tail, has been extensively studied and is understood as a universal feature of confined, single-file passive systems [2, 96–98]. To date, this power-law decay has not been reported for active systems. However, this behavior is not entirely unexpected, as prior work on single-file active systems has observed the characteristic subdiffusive behavior ( $\langle(\Delta x)^2\rangle \sim t^{1/2}$ ) [74, 99], which suggests that the velocity autocorrelation function must decay as  $-t^{-3/2}$ .

## DISCUSSION

In principle, the key quantity required to calculate the MSD is the velocity autocorrelation function, or equivalently, the normalized velocity autocorrelation function  $\mathcal{V}(\tau)$ , and the mean squared velocity  $\langle v^2 \rangle$ , as expressed in Eq. (9). Even in the case of passive systems, it is a challenge to derive an analytical expression for the velocity autocorrelation function that is quantitative across all time scales for interacting many-body systems [100, 101]. We direct the reader to various empirical and first-principle approaches proposed for passive systems to capture features of the velocity autocorrelation function [102]. However, even without full knowledge of the normalized velocity autocorrelation function for the interacting SF-ABP system, a quantitative understanding of the MSD's short-time behavior can be obtained. As the mean squared velocity is related to the reduced kinetic temperature via  $\langle v^2 \rangle = \frac{1}{2}U_a^2\mathcal{T}_k$ , substituting this expression into Eq. (9) gives:

$$\langle(\Delta x)^2\rangle = U_a^2\mathcal{T}_k t \left[ \int_0^t \left(1 - \frac{\tau}{t}\right) \mathcal{V}(\tau) d\tau \right]. \quad (11)$$

A zeroth-order approximation for the normalized velocity autocorrelation function (i.e.,  $\mathcal{V}(\tau) = 1$ ) and subsequent integration of Eq. (11), reveals that for all packing fractions and Péclet numbers, the motion of the particle is ballistic at short times, scaling as

$$\langle(\Delta x)^2\rangle \sim \frac{1}{2}U_a^2\mathcal{T}_k t^2 = \tau_R^{-1}D_0\mathcal{T}_k t^2. \quad (12)$$

In Fig. 4(a), we show that the short-time ballistic behavior of the MSD collapses onto a universal curve by appropriately rescaling by  $\mathcal{T}_k$ . Here, we arrive at a key observation: the MSD of a tagged ABP in the single-file system is always ballistic for times less than  $\tau_R$ , and the reduced kinetic temperature can quantitatively capture the particle's speed in this regime.

In an attempt to capture the short-time behavior of the normalized velocity autocorrelation function, we approximate the collisional force  $F_c$  to first order as  $F_c = -\kappa\Delta x$ , where  $\kappa$  represents a generalized spring constant. We envision that the presence of neighboring particles induces a caging effect, which we approximate by a harmonic potential. Within this harmonic approximation for  $F_c$ , the

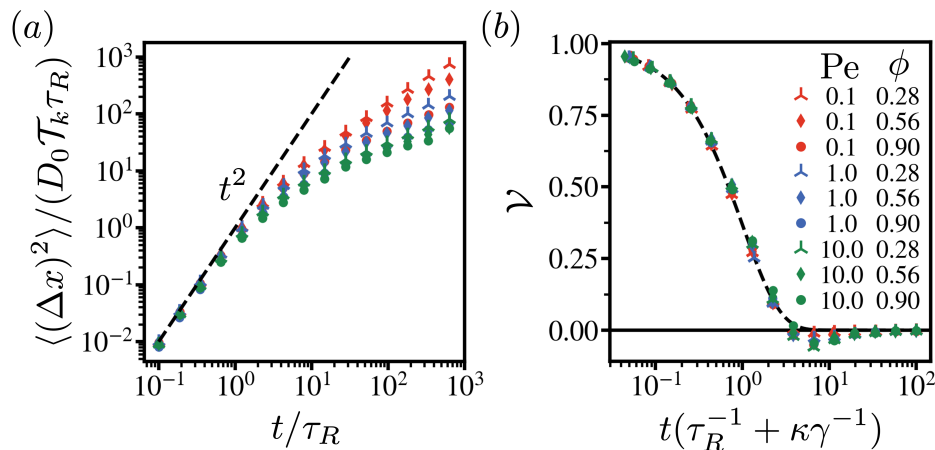


FIG. 4. (a) Universal collapse of the ballistic regime of the MSD when appropriately rescaled by the kinetic temperature [See Eq. (12)]. (b) Short-time collapse of the normalized velocity autocorrelation function, where the black line corresponds to the analytical result  $\mathcal{V}(t) = e^{-t(\tau_R^{-1} + \kappa\gamma^{-1})}$ .

normalized velocity autocorrelation function can be expressed as:

$$\mathcal{V}(t) = \frac{1}{1 - \tau_R \kappa \gamma^{-1}} \left( e^{-t/\tau_R} - e^{-t\kappa/\gamma} \right) + e^{-t\kappa/\gamma}. \quad (13)$$

Focusing on the short-time behavior, we expand Eq. (13) to first order, obtaining  $\mathcal{V}(t) = 1 - (\tau_R^{-1} + \kappa\gamma^{-1})t + \mathcal{O}(t^2) \approx e^{-t(\tau_R^{-1} + \kappa\gamma^{-1})}$ . For the functional form of the generalized spring constant, we construct a heuristic approximation  $\kappa \sim \gamma U_a \sqrt{\mathcal{T}_k} / \lambda_{ABP}$ , by identifying the relevant force scale acting on a tagged particle,  $\gamma U_a \sqrt{\mathcal{T}_k}$ , and the length scale over which the force acts given by the mean free path  $\lambda_{ABP}$ . The functional form of the generalized spring constant  $\kappa$  captures the following trends: As the packing fraction increases,  $\kappa$  increases, reflecting a more pronounced caging effect at higher packing fractions where particle collisions are more frequent. Conversely, as the active Péclet number increases at a fixed packing fraction,  $\kappa$  decreases, indicating that particles with greater persistence overcome the caging effect from their neighbors more easily. In Fig. 4(b), we demonstrate that the short-time behavior of the normalized velocity autocorrelation function is well captured by  $\mathcal{V}(t) = e^{-t(\tau_R^{-1} + \kappa\gamma^{-1})}$ , successfully reflecting the key trends in activity and packing fraction at short times. This form for the normalized velocity autocorrelation function in Eq. (11) provides a first-order correction to the MSD at short times. However, this expression does not capture the long-time behavior, particularly the power-law decay observed in the velocity autocorrelation function at later times.

To further rationalize the observed trends in the MSD, we introduce the corresponding Smoluchowski equation, which governs the time evolution of the probability density function (PDF) for a tagged ABP's position and ori-

entation. This conservation equation, which is formally equivalent to the equations of motion given in Eq. (4), is expressed as:

$$\partial_t P = -U_a \cos \theta \partial_x P - \frac{1}{\gamma} \partial_x (F_c P) + \frac{1}{\tau_R} \partial_{\theta\theta} P, \quad (14)$$

where  $P = P(x, \theta, t | x_0, \theta_0, t_0)$  is the probability of finding a tagged ABP at position  $x$  and orientation  $\theta$  at time  $t$ , given that it was at position  $x_0$  and orientation  $\theta_0$  at an earlier time  $t_0$ . The PDF satisfies the normalization condition  $\int dx d\theta P = 1$ , and we assume an initial condition of  $P(x_0, \theta_0, t_0) = \delta(x - x_0)/(2\pi)$ , where the ABP is initially localized at  $x_0$  with a uniform distribution in its orientation. Without loss of generality, we set  $x_0 = 0$  and  $t_0 = 0$ . The ensemble average of any microscopic observable  $f[x(t), \theta(t)]$  is then defined as:

$$\langle f[x(t), \theta(t)] \rangle = \int dx d\theta f(x, \theta) P(x, \theta, t | x_0, \theta_0, t_0).$$

Following a similar approach to Schakenraad et al. [103], we express the time derivative of the MSD as:

$$\partial_t \langle (\Delta x)^2 \rangle = \int dx d\theta (\Delta x)^2 \partial_t P, \quad (15)$$

which, upon substituting Eq. (14) into the right-hand side of Eq. (15), gives:

$$\partial_t \langle (\Delta x)^2 \rangle = \frac{2}{\gamma} \left[ \langle \Delta x F_a \rangle + \langle \Delta x F_c \rangle \right], \quad (16)$$

where the time derivative of the MSD is expressed in terms of two correlations:  $\langle \Delta x F_a \rangle$  and  $\langle \Delta x F_c \rangle$ . Interestingly, we show that the short-time ballistic behavior of the MSD is primarily governed by the correlation  $\langle \Delta x F_a \rangle$  and the long-time subdiffusive behavior is due to  $\langle \Delta x F_c \rangle$ .

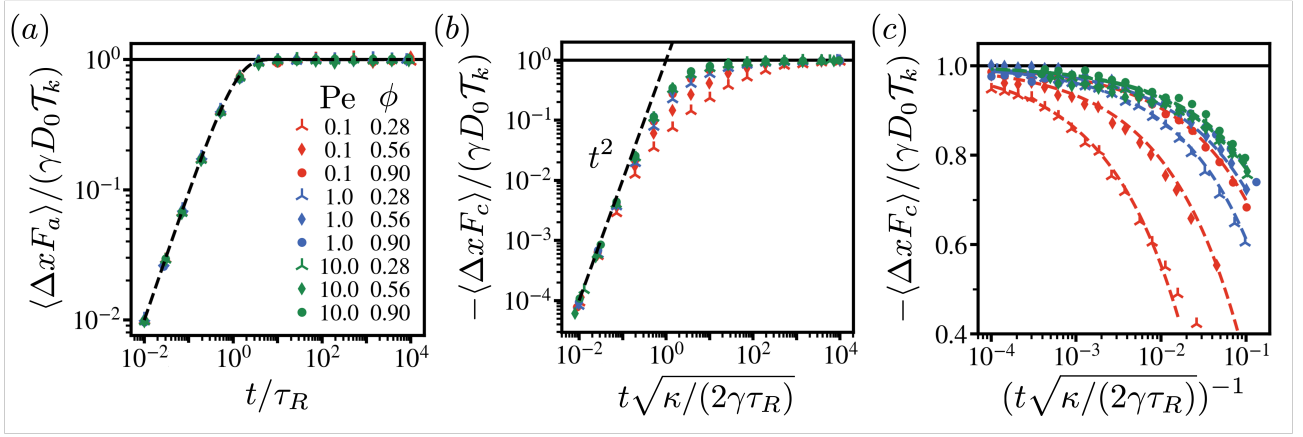


FIG. 5. Correlation (a)  $\langle \Delta x F_a \rangle$  and (b)  $\langle \Delta x F_c \rangle$  as measured from simulation for the representative set of Pe and  $\phi$ . The dashed black line in (a) corresponds to the analytical solution for  $\langle \Delta x F_a \rangle$  [Eq. (20)]. In (b), the dashed black line corresponds to the short-time scaling. The long-time behavior (c) is illustrated using colored lines which correspond to Eq. (22).

Additionally, in the asymptotic limit, the left-hand side of Eq. (16) vanishes as

$$\lim_{t \rightarrow \infty} \partial_t \langle (\Delta x)^2 \rangle \sim t^{-\frac{1}{2}} \rightarrow 0$$

establishing the long-time relationship:

$$\lim_{t \rightarrow \infty} \langle \Delta x F_a \rangle = \lim_{t \rightarrow \infty} -\langle \Delta x F_c \rangle. \quad (17)$$

We proceed by deriving analytical expressions for  $\langle \Delta x F_a \rangle$  and  $\langle \Delta x F_c \rangle$ , which allow us to obtain the MSD by integrating Eq. (16). We first express the time derivative of  $\langle \Delta x F_a \rangle$  as

$$\partial_t \langle \Delta x F_a \rangle = \frac{\gamma U_a^2}{2} + \frac{1}{\gamma} \langle F_a F_c \rangle - \frac{1}{\tau_R} \langle \Delta x F_a \rangle \quad (18)$$

using the same approach to derive Eq. (16). The correlation  $\langle F_a F_c \rangle$ , which is time independent, can be written in terms of the reduced kinetic temperature as

$$\langle F_a F_c \rangle = -\langle F_c^2 \rangle = -\frac{(\gamma U_a)^2}{2} (1 - \mathcal{T}_k), \quad (19)$$

where we have used Eq. (5) and the unique property of ABPs  $\langle v F_c \rangle = 0$  [77]. Upon substituting Eq. (19) into Eq. (18), we obtain the first-order differential equation

$$\partial_t \langle \Delta x F_a \rangle = \frac{\gamma U_a^2}{2} \mathcal{T}_k - \frac{1}{\tau_R} \langle \Delta x F_a \rangle, \quad (20)$$

with solution

$$\langle \Delta x F_a \rangle = \gamma D_0 \mathcal{T}_k \left[ 1 - e^{-t/\tau_R} \right]. \quad (21)$$

In Fig. 5(a), we show excellent agreement between Eq. (21) and simulation results demonstrating that all  $\phi$  and Pe values collapse onto a universal curve. By integrating Eq. (21), we obtain the predominant short-time

contribution to the MSD. We emphasize that Eq. (21) can be trivially extended to ABP in higher dimensions. However, in these higher dimensional systems, the Pe and  $\phi$  dependence of the reduced kinetic temperature has not been fully quantified.

The correlation  $\langle \Delta x F_c \rangle$  presents a greater challenge to calculate analytically due to the spatiotemporal complexity of the interparticle force  $F_c$ . Rather than providing an exact treatment, we perform a scaling analysis for both the short- and long-time behavior, which is sufficient to obtain an accurate expression for the MSD. Figure 5(b) presents simulation results for  $\langle \Delta x F_c \rangle$  over the representative range of  $\phi$  and Pe. At short times, all curves exhibit similar scaling behavior that is captured by our harmonic approximation for  $F_c$ , which gives the correct scaling  $\langle \Delta x F_c \rangle = -\kappa \langle (\Delta x)^2 \rangle \sim -\kappa D_0 \mathcal{T}_k t^2 / \tau_R$  for times less than  $\tau_R$ . The short-time behavior collapses onto a universal curve when scaled by the timescale  $\sqrt{(2\gamma\tau_R)/\kappa}$ , as shown in Fig. 5(b) (see Supplementary Material for calculation details [104]). The quadratic scaling of  $\langle \Delta x F_c \rangle$  at short times confirms that its contribution to the MSD is nominal. At short times,  $\langle \Delta x F_a \rangle$  contributes a ballistic term to the MSD, which grows more rapidly in time than the contribution from  $\langle \Delta x F_c \rangle$ , which scales as  $\langle (\Delta x)^2 \rangle \sim t^3$ . At long times,  $\langle \Delta x F_c \rangle$  plateaus to  $-\gamma D_0 \mathcal{T}_k$ , consistent with the asymptotic relationships derived in Eqs. (17) and (21), where

$$\lim_{t \rightarrow \infty} \langle \Delta x F_c \rangle = -\lim_{t \rightarrow \infty} \langle \Delta x F_a \rangle = -\gamma D_0 \mathcal{T}_k.$$

To bridge the short- and long-time regimes, we estimate the intermediate-time behavior of  $\langle \Delta x F_c \rangle$  by rewriting Eq. (16) as

$$\begin{aligned} \lim_{t \gg \tau_R} \langle \Delta x F_c \rangle &= \lim_{t \gg \tau_R} \left[ \frac{\gamma}{2} \partial_t \langle (\Delta x)^2 \rangle - \langle \Delta x F_a \rangle \right] \\ &= \frac{\gamma F}{2t^{1/2}} - \gamma D_0 \mathcal{T}_k. \end{aligned} \quad (22)$$

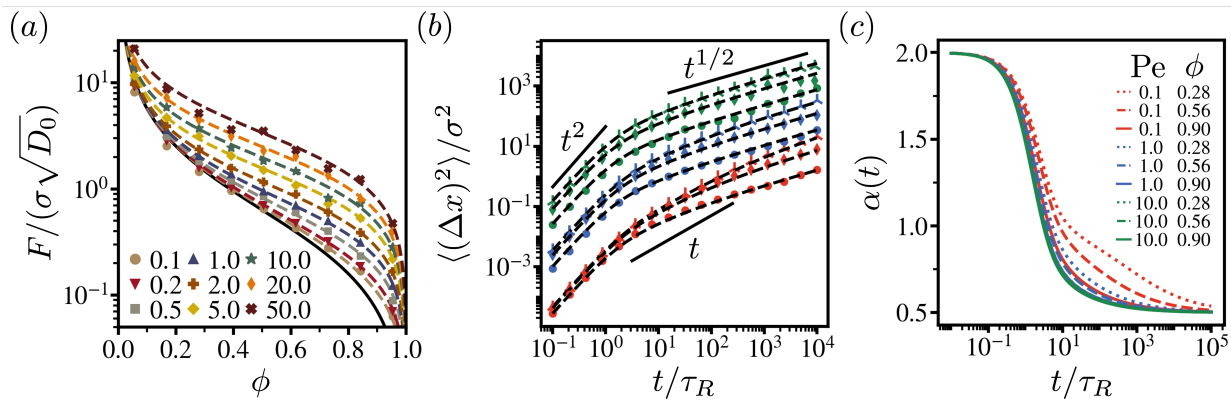


FIG. 6. (a) 1D-mobility for the SF-ABP system as a function of packing fraction for different active Péclet numbers. Simulation results are plotted as points and the analytical expression, Eq. (22), is plotted as a dashed colored line. (b) Scaled MSD measurements of a tracer particle in the SF-ABP system for different active Péclet numbers and packing fractions. Simulation results are plotted using colored points and the analytical expression, Eq. (24), is shown using black dashed lines. The local exponent of the MSD for the representative selection of Pe and  $\phi$ .

The second line of Eq. (22) follows from two key observations. At sufficiently long times all packing fractions and Péclet numbers exhibit subdiffusive scaling, leading to  $\partial_t \langle(\Delta x)^2\rangle = F/t^{1/2}$ . In the Supplementary Material [104], we include an analytical calculation demonstrating this fact using an active variant of the Rouse model. The second observation follows from Eq. (21), where  $\langle\Delta x F_a\rangle = \gamma D_0 \mathcal{T}_k$  for times larger than  $\tau_R$ .

Interestingly, the 1D-mobility of the SF-ABP system can be predicted using Kollmann's result for equilibrium single-file systems,

$$F = \frac{1}{\rho} \sqrt{\frac{D_0 \mathcal{X}}{\pi}}, \quad (23)$$

where the only modification is that  $\mathcal{X}$  is given by the constant Pe compressibility [Eq. (8)], and  $D_0 = \frac{1}{2} U_a^2 \tau_R$ , the free diffusion coefficient of an ideal ABP. In Fig. 6(a), we demonstrate excellent agreement between the measured 1D-mobility from simulation and Eq. (23). Using this expression for the 1D-mobility, we show in Fig. 5(c) good agreement between the intermediate-time scaling of  $\langle\Delta x F_c\rangle$  [Eq. (22)] and simulation results.

Although derived for equilibrium Brownian particles, Kollmann's result for the 1D-mobility appears to apply to a broader class of particle dynamics. Kollmann's core insight was to relate a tagged particle's MSD in the long-time limit to the static structure factor, which can, in turn, be related to the system's isothermal compressibility [105]. Since the static structure factor is a purely mechanical quantity depending only on particle positions, this connection remains valid for non-equilibrium single-file systems, as long as the static structure factor remains well-defined. For ABPs, prior work has shown that the relationship between the static structure factor and the constant Pe compressibility mirrors that in equilibrium

systems [87]. These observations validate the extension of Kollmann's result to the 1D-mobility of ABPs. Further work is needed to address the scope of this result and determine whether it can be extended to an even more general class of non-equilibrium particle dynamics.

To construct an accurate expression for the MSD of the SF-ABP system, we adopt an approach similar to Lin et al. [31], where the ansatz for the MSD is expressed as

$$\frac{1}{\langle(\Delta x)^2\rangle} = \frac{1}{\langle(\Delta x)^2\rangle_{\text{short}}} + \frac{1}{\langle(\Delta x)^2\rangle_{\text{long}}}. \quad (24)$$

This form of the MSD [Eq. (24)] captures the short- and long-time behavior of the MSD and smoothly interpolates between these two regimes at intermediate times. We model the short-time contribution to the MSD as

$$\begin{aligned} \langle(\Delta x)^2\rangle_{\text{short}} &= \frac{2}{\gamma} \int_0^t dt' \langle\Delta x F_a\rangle \\ &= 2D_0 \mathcal{T}_k \left[ t + \tau_R \left( e^{-t/\tau_R} - 1 \right) \right], \end{aligned} \quad (25)$$

where  $\langle\Delta x F_a\rangle$  is given by Eq. (21). This contribution is identical to the MSD of an ideal ABP [Eq. (10)], except for the prefactor  $\mathcal{T}_k$ , which accounts for the reduction in particle speeds due to collisions. At short times, Eq. (24) predicts ballistic motion, scaling as  $\langle(\Delta x)^2\rangle \sim \frac{1}{2} U_a^2 \mathcal{T}_k t^2$ , consistent with both simulation results and the short-time expansion in Eq. (12). The long-time contribution to the MSD is given by

$$\begin{aligned} \langle(\Delta x)^2\rangle_{\text{long}} &= \frac{2}{\gamma} \int_0^t dt' (\langle\Delta x F_c\rangle + \langle\Delta x F_a\rangle) \\ &= \frac{2}{\gamma} \int_0^t dt' \left( \frac{\gamma F}{2\sqrt{t'}} - \gamma D_0 \mathcal{T}_k + \gamma D_0 \mathcal{T}_k \right) \\ &= 2F t^{1/2}, \end{aligned} \quad (26)$$



where  $\langle \Delta x F_c \rangle$  is given by Eq. (22) and  $\langle \Delta x F_a \rangle$  reaches its asymptotic value of  $\gamma D_0 \mathcal{T}_k$ . Essentially, at long times, it is only necessary to retain the subdiffusive contribution to the MSD. Combining the short- and long-time behaviors, we arrive at the full expression of the MSD:

$$\langle (\Delta x)^2 \rangle = \frac{2D_0 \mathcal{T}_k [t + \tau_R (e^{-t/\tau_R} - 1)]}{1 + D_0 \mathcal{T}_k [t + \tau_R (e^{-t/\tau_R} - 1)]} \frac{\phi}{\sigma_p} \sqrt{\frac{\pi}{D_0 \mathcal{X} t}}. \quad (27)$$

In Fig. 6(b), we compare Eq. (27) and simulation results for the selected values of Pe and  $\phi$  and find excellent agreement across all time scales. By design, the ansatz for the MSD captures the short- and long-time behavior, so it is not surprising we show good agreement in these regimes, as our scaling analysis accurately predicts these regimes. We find the performance of Eq. (27) at intermediate times more surprising, where the intrinsic interpolation from the MSD ansatz accurately captures the crossover between the ballistic and subdiffusive regime.

In Fig. 6(c), we calculate the local exponent  $\alpha = d \ln(\langle \Delta x^2 \rangle) / d \ln(t)$ , which quantifies the scaling exponent of the MSD as a function of time (i.e.,  $\langle \Delta x^2 \rangle \sim t^\alpha$ ). At short times  $\alpha \approx 2$  for all Pe and  $\phi$ , illustrating that the MSD is ballistic at short times. After times greater than approximately  $\tau_R$ , the local exponent decreases with a scaling that depends on Pe and  $\phi$ . The trends observed for the local exponent agree with the simple scaling arguments discussed in Fig. 3(b). For sufficiently large  $\phi$  and Pe values, the local exponent rapidly decays from  $\alpha = 2$  to  $\alpha = \frac{1}{2}$ , characteristic of the MSD transitioning directly from ballistic to subdiffusive behavior. For the case where the MSD exhibits diffusive character at intermediate times (i.e. when  $\phi$  and Pe are sufficiently small), the local exponent rapidly decreases from  $\alpha = 2$  to  $\alpha = 1$  within a time  $\tau_R$ , followed by a slower decay that can expand several decades to reach the asymptotic value of  $\alpha = \frac{1}{2}$ . A short-time expansion of the local exponent for the MSD shows the following short-time scaling behavior

$$\alpha(t) = 2 - \frac{t}{3\tau_R} - \frac{3\text{Pe}\mathcal{T}_k\phi\sqrt{\pi t^3}}{4\sqrt{2}\mathcal{X}\tau_R^3} + \mathcal{O}(t^2). \quad (28)$$

The second term of this expansion corresponds to the decay of  $\alpha$  driven by the intrinsic reorientation of the particle via rotational diffusion. In contrast, the third term can be associated with further reduction in  $\alpha$  due to collisions with neighboring particles which depends on both Pe and  $\phi$ . In the Supplementary Material, we include an additional plot for the local exponent of the MSD for different values of Pe and  $\phi$ , illustrating how the crossover between various scaling regimes can be controlled. From an engineering and applications perspective, Eq. (27) encapsulates a design rule for obtaining a desired profile for the MSD of a tagged ABP, where it is possible to tune both the overall magnitude of the MSD and the duration of the various scaling regimes.

## CONCLUSION

This study characterizes the single-file diffusion (SFD) of active Brownian particles (ABPs) using a combination of Brownian dynamics simulations and analytical theory. Using scaling and heuristic arguments, we derived an accurate analytical expression for the mean square displacement (MSD) of a tagged ABP [Eq. (27)] as a function of Pe and  $\phi$ . Additionally, we demonstrated that Kollmann's 1D-mobility expression [Eq. (23)], initially developed for equilibrium systems, can be extended to active systems with minimal modification, highlighting key similarities between passive and active single-file systems. While our analytical model effectively captures the essential dynamics, open questions remain. Future work could involve solving the correlation term  $\langle \Delta x F_c \rangle$  exactly, which may offer modest improvements in predicting the MSD. Moreover, finding an exact analytical solution to the governing Smoluchowski equation [Eq. (14)], if feasible, would allow for precise calculations of higher-order moments, further refining our understanding of positional and orientational dynamics in SFD systems.

Future studies will explore systems with more complex interparticle interactions, potentially revealing new scaling behaviors or emergent transport mechanisms. An important open question is how these results differ when the particles are capable of inducing interparticle torques on one another such as in magnetic or patchy particle systems. In addition, hydrodynamic interactions and specific self-propulsion mechanisms may significantly influence these findings. Another natural extension of this study involves investigating how the MSD changes as a function of the channel width. In passive systems, there has been shown to be a crossover from single-file to Fickian diffusion at a characteristic channel width [93, 106]. Such a study would systematically elucidate the differences between transport in passive and active systems under varying degrees of confinement. Such extensions have practical relevance for applications in confined environments, with implications for the design of advanced microfluidic systems, drug delivery platforms, and environmental sensing mechanisms. Finally, experimental studies of single-file active colloids could offer exciting opportunities to test these predictions and evaluate their practical impact.

---

\* [sam7808@psu.edu](mailto:sam7808@psu.edu)

- [1] A. L. Hodgkin and R. D. Keynes, The potassium permeability of a giant nerve fibre, *J. Physiol.* **128**, 61 (1955).
- [2] D. W. Jepsen, Dynamics of a simple many-body system of hard rods, *J. Math. Phys.* **6**, 405 (1965).
- [3] J. L. Lebowitz and J. K. Percus, Kinetic equations and density expansions: Exactly solvable, *Phys. Rev.* **155**, 122 (1967).

- [4] D. G. Levitt, Dynamics of a single-file pore: Non-fickian behavior, *Phys. Rev. A Gen. Phys.* **8**, 3050 (1973).
- [5] W. Stephan, B. Kleutsch, and E. Frehland, Rate theory models for ion transport through rigid pores. III. continuum vs discrete models in single file diffusion, *J. Theor. Biol.* **105**, 287 (1983).
- [6] K. Eskesen and H. H. Ussing, Single-file diffusion through  $k^+$  channels in frog skin epithelium, *J. Membr. Biol.* **91**, 245 (1986).
- [7] J. M. D. MacElroy and S.-H. Suh, Self-diffusion in single-file pores of finite length, *J. Chem. Phys.* **106**, 8595 (1997).
- [8] C. Rödenbeck, J. Kärger, and K. Hahn, Calculating exact propagators in single-file systems via the reflection principle, *Phys. Rev. E* **57**, 4382 (1998).
- [9] K. K. Mon and J. K. Percus, Self-diffusion of fluids in narrow cylindrical pores, *J. Chem. Phys.* **117**, 2289 (2002).
- [10] M. Kollmann, Single-file diffusion of atomic and colloidal systems: asymptotic laws, *Phys. Rev. Lett.* **90**, 180602 (2003).
- [11] K. Nelissen, V. R. Misko, and F. M. Peeters, Single-file diffusion of interacting particles in a one-dimensional channel, *Euro. Phys. Lett.* **80**, 56004 (2007).
- [12] L. Lizana and T. Ambjörnsson, Single-file diffusion in a box, *Phys. Rev. Lett.* **100**, 200601 (2008).
- [13] V. N. Kharkyanen and S. O. Yesylevskyy, Theory of single-file multiparticle diffusion in narrow pores, *Phys. Rev. E* **80**, 031118 (2009).
- [14] S. Herrera-Velarde, A. Zamudio-Ojeda, and R. Castañeda-Priego, Ordering and single-file diffusion in colloidal systems, *J. Chem. Phys.* **133**, 114902 (2010).
- [15] A. S. Stern and H. C. Berg, Single-file diffusion of flagellin in flagellar filaments, *Biophys. J.* **105**, 182 (2013).
- [16] N. Leibovich and E. Barkai, Everlasting effect of initial conditions on single-file diffusion, *Phys. Rev. E* **88**, 032107 (2013).
- [17] S. D. Goldt and E. M. Terentjev, Role of the potential landscape on the single-file diffusion through channels, *J. Chem. Phys.* **141**, 224901 (2014).
- [18] E. Locatelli, M. Pierno, F. Baldovin, E. Orlandini, Y. Tan, and S. Pagliara, Single-file escape of colloidal particles from microfluidic channels, *Phys. Rev. Lett.* **117**, 038001 (2016).
- [19] S. Farrell and A. D. Rutenberg, Non-fickian single-file pore transport, *Phys. Rev. E* **104**, L032102 (2021).
- [20] T. E. Harris, Diffusion with “collisions” between particles, *J. Appl. Probab.* **2**, 323 (1965).
- [21] D. G. Levitt, Dynamics of a single-file pore: Non-fickian behavior, *Phys. Rev. A* **8**, 3050 (1973).
- [22] M. Kollmann, Single-file diffusion of atomic and colloidal systems: asymptotic laws, *Phys. Rev. Lett.* **90**, 180602 (2003).
- [23] J. Kärger, Single-file diffusion in zeolites, in *Adsorption and Diffusion*, edited by H. G. Karge and J. Weitkamp (Springer Berlin Heidelberg, Berlin, Heidelberg, 2008) pp. 329–366.
- [24] B. U. Felderhof, Fluctuation theory of single-file diffusion, *J. Chem. Phys.* **131**, 064504 (2009).
- [25] P. M. Centres and S. Bustingorry, Effective edwards-wilkinson equation for single-file diffusion, *Phys. Rev. E Stat. Nonlin. Soft Matter Phys.* **81**, 061101 (2010).
- [26] F. Höfling and T. Franosch, Anomalous transport in the crowded world of biological cells, *Rep. Prog. Phys.* **76**, 046602 (2013).
- [27] H. Jobic, Observation of single-file diffusion in a MOF, *Phys. Chem. Chem. Phys.* **18**, 17190 (2016).
- [28] Q. Wei, C. Bechinger, and P. Leiderer, Single-file diffusion of colloids in one-dimensional channels, *Science* **287**, 625 (2000).
- [29] C. Lutz, M. Kollmann, and C. Bechinger, Single-file diffusion of colloids in one-dimensional channels, *Phys. Rev. Lett.* **93**, 026001 (2004).
- [30] C. Lutz, M. Kollmann, P. Leiderer, and C. Bechinger, Diffusion of colloids in one-dimensional light channels, *J. Phys. Condens. Matter* **16**, S4075 (2004).
- [31] B. Lin, M. Meron, B. Cui, S. A. Rice, and H. Diamant, From random walk to single-file diffusion, *Phys. Rev. Lett.* **94**, 216001 (2005).
- [32] C. Coste, J.-B. Delfau, C. Even, and M. Saint Jean, Single-file diffusion of macroscopic charged particles, *Phys. Rev. E* **81**, 051201 (2010).
- [33] A. Villada-Balbuena, A. Ortiz-Ambriz, P. Castro-Villarreal, P. Tierno, R. Castañeda-Priego, and J. M. Méndez-Alcaraz, Single-file dynamics of colloids in circular channels: Time scales, scaling laws and their universality, *Phys. Rev. Research* **3**, 033246 (2021).
- [34] V. Kukla, V. J. Kornatowski, D. Demuth, I. Girnus, I. H. Pfeifer, L. V. C. Rees, S. Schunk, K. K. Unger, and J. Karger, NMR studies of single-file diffusion in unidimensional channel zeolites, *Science* **272**, 702 (1996).
- [35] J. Kärger and D. M. Ruthven, Self-diffusion and diffusive transport in zeolite crystals, in *Studies in Surface Science and Catalysis*, Vol. 105, edited by H. Chon, S.-K. Ihm, and Y. S. Uh (Elsevier, 1997) pp. 1843–1850.
- [36] J. Kärger, Single-file diffusion in zeolites, in *Adsorption and Diffusion*, edited by H. G. Karge and J. Weitkamp (Springer Berlin Heidelberg, Berlin, Heidelberg, 2008) pp. 329–366.
- [37] Z. Li, R. P. Misra, Y. Li, Y.-C. Yao, S. Zhao, Y. Zhang, Y. Chen, D. Blankshtein, and A. Noy, Breakdown of the nernst-einstein relation in carbon nanotube porins, *Nat. Nanotechnol.* **18**, 177 (2023).
- [38] C. Boldrighini, R. L. Dobrushin, and Y. M. Sukhov, One-dimensional hard rod caricature of hydrodynamics, *J. Stat. Phys.* **31**, 577 (1983).
- [39] J. Bleibel, A. Domínguez, F. Günther, J. Harting, and M. Oettel, Hydrodynamic interactions induce anomalous diffusion under partial confinement, *Soft Matter* **10**, 2945 (2014).
- [40] P. Rizkallah, A. Grabsch, P. Illien, and O. Bénichou, Duality relations in single-file diffusion, *J. Stat. Mech.* **2023**, 013202 (2023).
- [41] A. Taloni and M. A. Lomholt, Langevin formulation for single-file diffusion, *Phys. Rev. E* **78**, 051116 (2008).
- [42] C. Eab and S. Lim, Fractional generalized langevin equation approach to single-file diffusion, *Physica A: Statistical Mechanics and its Applications* **389**, 2510 (2010).
- [43] A. Taloni and F. Marchesoni, Interacting single-file system: Fractional langevin formulation versus diffusion-noise approach, *Biophys. Rev. Lett.* **09**, 381 (2014).
- [44] D. Dürr, S. Goldstein, and J. L. Lebowitz, Asymptotics of particle trajectories in infinite one-dimensional systems with collisions, *Commun. Pure Appl. Math.* **38**, 573 (1985).
- [45] K. Hahn and J. Karger, Propagator and mean-square

- displacement in single-file systems, *J. Phys. A Math. Gen.* **28**, 3061 (1995).
- [46] O. Flomenbom and A. Taloni, On single-file and less dense processes, *Euro. Phys. Lett.* **83**, 20004 (2008).
- [47] M. A. Lomholt and T. Ambjörnsson, Universality and nonuniversality of mobility in heterogeneous single-file systems and rouse chains, *Phys. Rev. E* **89**, 032101 (2014).
- [48] A. Taloni, O. Flomenbom, R. Castañeda-Priego, and F. Marchesoni, Single file dynamics in soft materials, *Soft Matter* **13**, 1096 (2017).
- [49] O. Bénichou, P. Illien, G. Oshanin, A. Sarracino, and R. Voituriez, Tracer diffusion in crowded narrow channels, *J. Phys. Condens. Matter* **30**, 443001 (2018).
- [50] A. Santos, *A concise course on the theory of classical liquids: Basics and selected topics*, 1st ed., Lecture notes in physics (Springer International Publishing, Cham, Switzerland, 2016).
- [51] L. Lizana, T. Ambjörnsson, A. Taloni, E. Barkai, and M. A. Lomholt, Foundation of fractional langevin equation: harmonization of a many-body problem, *Phys. Rev. E* **81**, 051118 (2010).
- [52] G. S. Redner, M. F. Hagan, and A. Baskaran, Structure and dynamics of a phase-separating active colloidal fluid, *Phys. Rev. Lett.* **110**, 055701 (2013).
- [53] Y. Fily and M. C. Marchetti, Athermal phase separation of self-propelled particles with no alignment, *Phys. Rev. Lett.* **108**, 235702 (2012).
- [54] P. Illien, O. Bénichou, C. Mejía-Monasterio, G. Oshanin, and R. Voituriez, Active transport in dense diffusive single-file systems, *Phys. Rev. Lett.* **111**, 038102 (2013).
- [55] R. Soto and R. Golestanian, Run-and-tumble dynamics in a crowded environment: persistent exclusion process for swimmers, *Phys. Rev. E* **89**, 012706 (2014).
- [56] S. A. Mallory, C. Valeriani, and A. Cacciuto, Curvature-induced activation of a passive tracer in an active bath, *Phys. Rev. E* **90**, 032309 (2014).
- [57] S. A. Mallory, C. Valeriani, and A. Cacciuto, Anomalous dynamics of an elastic membrane in an active fluid, *Phys. Rev. E* **92**, 012314 (2015).
- [58] S. A. Mallory and A. Cacciuto, Activity-assisted self-assembly of colloidal particles, *Phys. Rev. E* **94**, 022607 (2016).
- [59] S. A. Mallory, F. Alarcon, A. Cacciuto, and C. Valeriani, Self-assembly of active amphiphilic janus particles, *New J. Phys.* **19**, 125014 (2017).
- [60] S. A. Mallory, C. Valeriani, and A. Cacciuto, An active approach to colloidal self-assembly, *Annu. Rev. Phys. Chem.* **69**, 59 (2018).
- [61] L. Barberis and F. Peruani, Phase separation and emergence of collective motion in a one-dimensional system of active particles, *J. Chem. Phys.* **150**, 144905 (2019).
- [62] S. A. Mallory and A. Cacciuto, Activity-enhanced self-assembly of a colloidal kagome lattice, *J. Am. Chem. Soc.* **141**, 2500 (2019).
- [63] S. A. Mallory, M. L. Bowers, and A. Cacciuto, Universal reshaping of arrested colloidal gels via active doping, *J. Chem. Phys.* **153**, 084901 (2020).
- [64] S. A. Mallory, A. K. Omar, and J. F. Brady, Dynamic overlap concentration scale of active colloids, *Phys. Rev. E* **104**, 044612 (2021).
- [65] A. K. Omar, H. Row, S. A. Mallory, and J. F. Brady, Mechanical theory of nonequilibrium coexistence and motility-induced phase separation, *Proc. Natl. Acad. Sci. U. S. A.* **120**, e2219900120 (2023).
- [66] S. Paul, A. Dhar, and D. Chaudhuri, Dynamical crossovers and correlations in a harmonic chain of active particles, *Soft Matter* (2024).
- [67] P. Bayati and S. A. Mallory, Orbits, spirals, and trapped states: Dynamics of a phoretic janus particle in a radial concentration gradient, *ACS Nano* **18**, 23047 (2024).
- [68] P. Romanczuk and U. Erdmann, Collective motion of active brownian particles in one dimension, *Eur. Phys. J. Spec. Top.* **187**, 127 (2010).
- [69] E. Locatelli, *Dynamical and collective properties of active and passive particles in Single File*, Ph.D. thesis, University of Padua (2014).
- [70] Y. Fily, A. Baskaran, and M. F. Hagan, Dynamics of self-propelled particles under strong confinement, *Soft Matter* **10**, 5609 (2014).
- [71] E. C. Euán-Díaz, S. Herrera-Velarde, V. R. Misko, F. M. Peeters, and R. Castañeda-Priego, Single-file diffusion of driven interacting colloids, *Biophys. Rev. Lett.* **09**, 413 (2014).
- [72] L. Alonso-Llanes, A. Garcimartín, and I. Zuriguel, Single file motion of robot swarms, *Phys. Rev. Res.* **6**, L022037 (2024).
- [73] K. Misiunas and U. F. Keyser, Density-dependent speed-up of particle transport in channels, *Phys. Rev. Lett.* **122**, 214501 (2019).
- [74] P. Dolai, A. Das, A. Kundu, C. Dasgupta, A. Dhar, and K. V. Kumar, Universal scaling in active single-file dynamics, *Soft Matter* **16**, 7077 (2020).
- [75] T. Banerjee, R. L. Jack, and M. E. Cates, Tracer dynamics in one dimensional gases of active or passive particles, arXiv [cond-mat.stat-mech] (2021).
- [76] S. Jose, First passage statistics of active random walks on one and two dimensional lattices, arXiv [cond-mat.stat-mech] (2022).
- [77] E. Schiltz-Rouse, H. Row, and S. A. Mallory, Kinetic temperature and pressure of an active tonks gas, *Phys. Rev. E* **108**, 064601 (2023).
- [78] J. D. Weeks, D. Chandler, and H. C. Andersen, Role of repulsive forces in determining the equilibrium structure of simple liquids, *J. Chem. Phys.* **54**, 5237 (1971).
- [79] J. A. Anderson, J. Glaser, and S. C. Glotzer, HOOMD-blue: A python package for high-performance molecular dynamics and hard particle monte carlo simulations, *Comput. Mater. Sci.* **173**, 109363 (2020).
- [80] L. Tonks, The complete equation of state of one, two and three-dimensional gases of hard elastic spheres, *Phys. Rev.* **50**, 955 (1936).
- [81] C. M. B. Gutiérrez, C. Vanhille-Campos, F. Alarcón, I. Pagonabarraga, R. Brito, and C. Valeriani, Collective motion of run-and-tumble repulsive and attractive particles in one-dimensional systems, *Soft Matter* **17**, 10479 (2021).
- [82] T. Debnath, S. Nayak, P. Bag, D. Debnath, and P. K. Ghosh, Structure and diffusion of active-passive binary mixtures in a single-file, *J. Chem. Sci. (Bangalore)* **135**, 38 (2023).
- [83] N. Sepúlveda and R. Soto, Coarsening and clustering in run-and-tumble dynamics with short-range exclusion, *Phys. Rev. E* **94**, 022603 (2016).
- [84] P. de Castro, S. Diles, R. Soto, and P. Sollich, Active mixtures in a narrow channel: motility diversity changes cluster sizes, *Soft Matter* **17**, 2050 (2021).

- [85] E. Locatelli, F. Baldovin, E. Orlandini, and M. Pierno, Active brownian particles escaping a channel in single file, *Phys. Rev. E* **91**, 022109 (2015).
- [86] I. Mukherjee, A. Raghu, and P. K. Mohanty, Nonexistence of motility induced phase separation transition in one dimension, *SciPost Phys.* **14**, 165 (2023).
- [87] A. R. Dulaney, S. A. Mallory, and J. F. Brady, The “isothermal” compressibility of active matter, *J. Chem. Phys.* **154**, 014902 (2021).
- [88] M. D. Graham, *Cambridge texts in applied mathematics: Microhydrodynamics, Brownian motion, and complex fluids series number 58* (Cambridge University Press, Cambridge, England, 2018).
- [89] B. ten Hagen, S. van Teeffelen, and H. Lowen, Non-gaussian behaviour of a self-propelled particle on a substrate, *Condensed Matter Physics* **12**, 725 (2009).
- [90] T. Ooshida, S. Goto, T. Matsumoto, and M. Otsuki, Insights from single-file diffusion into cooperativity in higher dimensions, *Biophys. Rev. Lett.* **11**, 9 (2016).
- [91] R. Wittmann, H. Löwen, and J. M. Brader, Order-preserving dynamics in one dimension – single-file diffusion and caging from the perspective of dynamical density functional theory, *Mol. Phys.* **119**, e1867250 (2021).
- [92] J. M. Rallison, Brownian diffusion in concentrated suspensions of interacting particles, *J. Fluid Mech.* **186**, 471–500 (1988).
- [93] J. Sané, J. T. Padding, and A. A. Louis, The crossover from single file to fickian diffusion, *Faraday Discuss.* **144**, 285 (2010).
- [94] S. Schweers, A. P. Antonov, A. Ryabov, and P. Maass, Scaling laws for single-file diffusion of adhesive particles, *Phys. Rev. E* **107**, L042102 (2023).
- [95] A. K. Tripathi and D. Kumar, Velocity correlations and mobility in single-file diffusion, *Phys. Rev. E* **81**, 021125 (2010).
- [96] H. Dekker, Long-time tail in velocity correlations in a one-dimensional rayleigh gas, *Phys. Lett. A* **88**, 21 (1982).
- [97] M. H. J. Hagen, I. Pagonabarraga, C. P. Lowe, and D. Frenkel, Algebraic decay of velocity fluctuations in a confined fluid, *Phys. Rev. Lett.* **78**, 3785 (1997).
- [98] J. Stepišnik and P. T. Callaghan, The long time tail of molecular velocity correlation in a confined fluid: observation by modulated gradient spin-echo NMR, *Physica B Condens. Matter* **292**, 296 (2000).
- [99] T. Bertrand, P. Illien, O. Bénichou, and R. Voituriez, Dynamics of run-and-tumble particles in dense single-file systems, *New J. Phys.* **20**, 113045 (2018).
- [100] D. McQuarrie, *Statistical Mechanics*, G - Reference, Information and Interdisciplinary Subjects Series (University Science Books, 2000).
- [101] B. Berne and R. Pecora, *Dynamic Light Scattering: With Applications to Chemistry, Biology, and Physics*, Dover Books on Physics (Dover Publications, 2013).
- [102] J. Boon and S. Yip, *Molecular Hydrodynamics*, Dover books on physics (Dover Publications, 1991).
- [103] K. Schakenraad, L. Ravazzano, N. Sarkar, J. A. J. Woutergem, R. M. H. Merks, and L. Giomi, Topotaxis of active brownian particles, *Phys. Rev. E* **101**, 032602 (2020).
- [104] See Supplemental Material at [URL] for details.
- [105] P. N. Pusey and R. J. A. Tough, Particle interactions, in *Dynamic Light Scattering*, edited by R. Pecora (Springer US, Boston, MA, 1985) pp. 85–179.
- [106] K. K. Mon and J. K. Percus, Pore-size dependence of quasi-one-dimensional single-file diffusion mobility, *J. Phys. Chem. C Nanomater. Interfaces* **111**, 15995 (2007).

# Supplemental Material: Single-File Diffusion of Active Brownian Particles

Akinlade Akintunde,<sup>1</sup> Parvin Bayati,<sup>1</sup> Hyeongjoo Row,<sup>2</sup> and Stewart A. Mallory<sup>1,3,\*</sup>

<sup>1</sup>Department of Chemistry, The Pennsylvania State University, University Park, Pennsylvania, 16802, USA

<sup>2</sup>Department of Chemical and Biomolecular Engineering, UC Berkeley, Berkeley, CA 94720, USA

<sup>3</sup>Department of Chemical Engineering, The Pennsylvania State University, University Park, Pennsylvania, 16802, USA

(Dated: November 15, 2024)

## SHORT TIME QUADRATIC BEHAVIOR OF $\langle \Delta x F_c \rangle$

Within the harmonic approximation for the collisional force ( $F_c = -\kappa \Delta x$ ) and using the same technique to derive Eqs. (16) and (18) of the main text, we can express the time derivative of  $\partial_t \langle \Delta x F_c \rangle$  as

$$\partial_t \langle \Delta x F_c \rangle = -\kappa \partial_t \langle (\Delta x)^2 \rangle = -\frac{2\kappa}{\gamma} \left[ \langle \Delta x F_a \rangle + \langle \Delta x F_c \rangle \right]. \quad (S1)$$

Multiplying both sides by  $e^{2\kappa t/\gamma}$  gives

$$e^{2\kappa t/\gamma} \partial_t \langle \Delta x F_c \rangle + \frac{2\kappa}{\gamma} e^{2\kappa t/\gamma} \langle \Delta x F_c \rangle = -\frac{2\kappa}{\gamma} \langle \Delta x F_a \rangle e^{2\kappa t/\gamma}, \quad (S2)$$

which simplifies to

$$\partial_t (e^{2\kappa t/\gamma} \langle \Delta x F_c \rangle) = -\frac{2\kappa}{\gamma} \langle \Delta x F_a \rangle e^{2\kappa t/\gamma}. \quad (S3)$$

The expression above can be integrated and rearranged to obtain

$$\langle \Delta x F_c \rangle = -\frac{2\kappa}{\gamma} e^{-2\kappa t/\gamma} \int_0^t d\tau \langle \Delta x F_a \rangle e^{2\kappa \tau/\gamma}, \quad (S4)$$

and substitution of  $\langle \Delta x F_a \rangle$  from Eq. (21) of the main text gives

$$\langle \Delta x F_c \rangle = -\frac{\gamma D_0 \mathcal{T}_k}{1 - (2\kappa \tau_R)/\gamma} \left[ 1 - e^{-\frac{2\kappa}{\gamma} t} - \frac{2\kappa \tau_R}{\gamma} \left( 1 - e^{-t/\tau_R} \right) \right]. \quad (S5)$$

A short time expansion of this expression gives  $\langle \Delta x F_c \rangle \sim -\kappa D_0 \mathcal{T}_k t^2/\tau_R$ , illustrating the quadratic scaling at short times and the timescale  $\sqrt{(2\gamma\tau_R)/\kappa}$  used to obtain the collapse in Fig. 5(b) of the main text.

## LONG TIME BEHAVIOR OF THE MEAN SQUARE DISPLACEMENT (ACTIVE ROUSE MODEL)

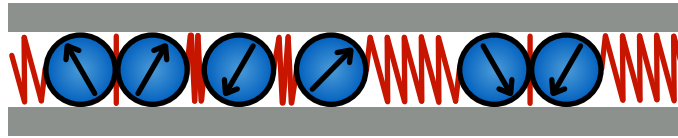


FIG. S1. Schematic of active Rouse SF-ABP system where interparticle interactions are modeled as springs. Each purely repulsive active particle moves at a constant speed of  $U_a \cos \theta$  while undergoing rotational Brownian motion with a reorientation time of  $\tau_R$ .

In this calculation, we model the SF-ABP system as an active variant of the Rouse Model, where active Brownian particles are bonded via harmonic springs in a one-dimensional geometry. A schematic illustrating the model is shown in Fig. S1. Within the context of this model, the equation of motion of a tagged ABP or “monomer” can be written as [1–3],

$$v(n, t) = \partial_t x(n, t) = \gamma^{-1} F_a(n, t) + \gamma^{-1} k [x(n+1, t) + x(n-1, t) - 2x(n, t)], \quad (S6)$$



where  $x(n, t)$  is the position of the tagged particle ( $n^{\text{th}}$  particle) at time  $t$  with its initial position set to zero,  $x(n, t = 0) = 0$  and  $k$  is the strength of the spring constant between adjacent ABPs. To match the geometry of the SF-ABP system studied in the main text, we consider a one-dimensional periodic system of length  $2L$  where the first and last particles in the channel are bonded. We work in the limit where both the length of the channel and the number of particles are large, but the ratio  $N/L$  remains finite. In this continuum limit, we define the Fourier-Laplace transform of the particle position as,

$$\hat{x}(q, s) = \int_{-\infty}^{\infty} dn \int_0^{\infty} dt e^{-iqn} e^{-st} x(n, t), \quad (\text{S7})$$

with inverse transform,

$$x(n, t) = \frac{1}{4\pi^2 i} \int_{-\infty}^{\infty} dq \int_{c-i\infty}^{c+i\infty} ds e^{iqn} e^{st} \hat{x}(q, s), \quad (\text{S8})$$

where  $c$  is a real number greater than the real part of all singularities of  $\hat{x}(q, s)$ . Using a second-order centered difference scheme and applying the Fourier-Laplace transform, Eq. (S1) can be rewritten as

$$s\hat{x}(q, s) = \gamma^{-1} \hat{F}_a(q, s) - \gamma^{-1} k q^2 \hat{x}(q, s). \quad (\text{S9})$$

From Eq. (S5), we can compute the translational autocorrelation function of a particle in Fourier-Laplace space,

$$\langle \hat{x}(q_1, s_1) \hat{x}(q_2, s_2) \rangle = \frac{\langle \hat{F}_a(q_1, s_1) \hat{F}_a(q_2, s_2) \rangle}{(\gamma s_1 + k q_1^2)(\gamma s_2 + k q_2^2)}, \quad (\text{S10})$$

where  $\langle \hat{F}_a(q_1, s_1) \hat{F}_a(q_2, s_2) \rangle$  is the Fourier-Laplace transform of the active force autocorrelation function [4, 5],

$$\langle F_a(n_1, t_1) F_a(n_2, t_2) \rangle = \frac{1}{2} (\gamma U_a)^2 e^{-|t_1 - t_2|/\tau_R} \delta(n_1 - n_2). \quad (\text{S11})$$

The Dirac delta function  $\delta(n_1 - n_2)$  is included to reflect the fact that active forces between different particles are completely uncorrelated. In the long time limit, the autocorrelation of the active force can be assumed to be delta correlated and Eq. (S11) can be rewritten as

$$\langle F_a(n_1, t_1) F_a(n_2, t_2) \rangle \approx \frac{1}{2} (\gamma U_a)^2 \delta(t_1 - t_2) \delta(n_1 - n_2). \quad (\text{S12})$$

The Fourier-Laplace transform of  $\langle F_a(n_1, t_1) F_a(n_2, t_2) \rangle$  gives

$$\langle \hat{F}_a(q_1, s_1) \hat{F}_a(q_2, s_2) \rangle = \frac{\pi (\gamma U_a)^2 \delta(q_2 + q_1)}{s_1 + s_2}. \quad (\text{S13})$$

Equation (S13) can be substituted into Eq. (S10) to obtain an expression for the positional autocorrelation function

$$\langle \hat{x}(q_1, s_1) \hat{x}(q_2, s_2) \rangle = \frac{\pi U_a^2 \delta(q_2 + q_1)}{(s_1 + s_2)(s_1 + k q_1^2 \gamma^{-1})(s_2 + k q_2^2 \gamma^{-1})}. \quad (\text{S14})$$

In order to obtain this autocorrelation function in real space and time, we first take the inverse Laplace transform

$$\langle \tilde{x}(q_1, t_1) \tilde{x}(q_2, t_2) \rangle = -\frac{1}{4\pi^2} \int_{c-i\infty}^{c+i\infty} ds_1 e^{s_1 t_1} \int_{c'-i\infty}^{c'+i\infty} ds_2 e^{s_2 t_2} \langle \hat{x}(q_1, s_1) \hat{x}(q_2, s_2) \rangle. \quad (\text{S15})$$

Both integration here can be evaluated by rewriting the expression as a limit of contour integrals. We first calculate the integral over  $s_2$  and assume without loss of generality that  $s_2 < s_1$  and  $t_2 < t_1$ . The contour shown in Fig. S2 (assuming  $t_2 > 0$ ) is used to evaluate the following contour integrals

$$\oint_{\Omega} dz F(z) = \int_{\Omega_1} dz F(z) + \int_{\Omega_2} dz F(z) = 2\pi i \sum_{z=z_i}^2 \text{Res } F(z), \quad (\text{S16})$$

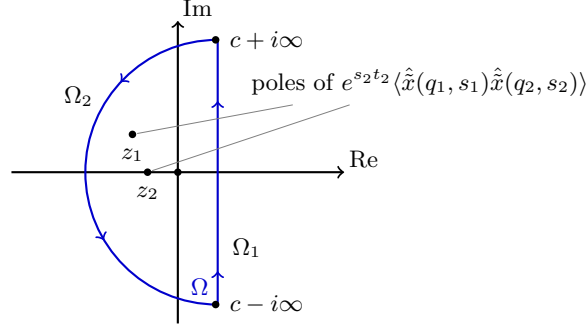


FIG. S2. Integration contour in the complex plane corresponding to Eq. (S15)

where the integrand  $F(z) = e^{tz} \langle \hat{x}(q_1, s_1) \hat{x}(q_2, z) \rangle$  has two first-order poles (singularities) at  $z_1 = -s_1$ ,  $z_2 = -kq_2^2 \gamma^{-1}$ , and  $\text{Res}_{z=z_i} F(z)$  represents the residue of  $F(z)$  at the pole  $z = z_i$ . The chosen contour  $\Omega$  allows the integral over the curved arc  $\Omega_2$  to vanish due to Jordans's lemma for  $t_2 > 0$ . Thus, the integral over  $\Omega_1$  is of primary interest and equals the sum of the residues as follows

$$\int_{\Omega_1} dz F(z) = \int_{c-i\infty}^{c+i\infty} ds_2 e^{s_2 t_2} \langle \hat{x}(q_1, s_1) \hat{x}(q_2, s_2) \rangle = 2\pi i \sum_{i=1}^2 \text{Res}_{z=z_i} F(z). \quad (\text{S17})$$

The residue of the integrand  $F(z)$  at any pole  $z_i$  is given by

$$\text{Res}_{z=z_i} F(z) = \frac{\phi^{(m-1)}(z_i)}{(m-1)!}, \quad (\text{S18})$$

where  $m$  is the order of the pole and  $\phi(z) = F(z_i)(z - z_i)^m$ . Here,  $\phi^{(m)}(z_i)$  is the  $m^{\text{th}}$  derivative of  $\phi$  with respect to  $z$  at  $z = z_i$ . Using contour integration, we evaluate the integral over  $s_2$  to obtain,

$$\int_{c-i\infty}^{c+i\infty} ds_2 e^{s_2 t_2} \langle \hat{x}(q_1, s_1) \hat{x}(q_2, s_2) \rangle = \frac{2\pi^2 i U_a^2 \delta(q_2 + q_1)}{(s_1 + kq_1^2 \gamma^{-1})(s_1 - kq_2^2 \gamma^{-1})} (e^{-kq_2^2 t_2 \gamma^{-1}} - e^{-s_1 t_2}), \quad (\text{S19})$$

and can rewrite Eq. (S15) as

$$\langle \tilde{x}(q_1, t_1) \tilde{x}(q_2, t_2) \rangle = \frac{U_a^2 \delta(q_2 + q_1)}{2i} \int_{c-i\infty}^{c+i\infty} ds_1 \frac{e^{s_1 t_1} e^{-kq_2^2 t_2 \gamma^{-1}} - e^{s_1 |t_1 - t_2|}}{(s_1 + kq_1^2 \gamma^{-1})(s_1 - kq_2^2 \gamma^{-1})}. \quad (\text{S20})$$

In our results, we assume the system is at a steady state and, therefore, exhibits time-translation invariance. We include the absolute value of  $t_1 - t_2$  to capture this fact and to ensure that the solution remains invariant under the order of integration over  $s_1$  and  $s_2$ . We also recognize that the integration in Eq. (S20) can be evaluated using a similar procedure. Here, the integrand is redefined as

$$F(z) = \frac{e^{z t_1} e^{-kq_2^2 t_2 \gamma^{-1}} - e^{z |t_1 - t_2|}}{(z + kq_1^2 \gamma^{-1})(z - kq_2^2 \gamma^{-1})},$$

and has two real first-order poles at  $z_1 = -kq_1^2 \gamma^{-1}$ ,  $z_2 = kq_2^2 \gamma^{-1}$ . The integration over  $\Omega_2$  vanishes due to Jordans's lemma for  $t_1 > 0$  and  $|t_1 - t_2| > 0$ , and again integration over  $\Omega_1$  is of primary interest. The integration over  $\Omega_1$  is equal to the sum of the residues

$$\int_{\Omega_1} dz F(z) = \int_{c-i\infty}^{c+i\infty} ds_1 \frac{e^{s_1 t_1} e^{-kq_2^2 t_2 \gamma^{-1}} - e^{s_1 |t_1 - t_2|}}{(s_1 + kq_1^2 \gamma^{-1})(s_1 - kq_2^2 \gamma^{-1})} = 2\pi i \sum_{i=1}^2 \text{Res}_{z=z_i} F(z), \quad (\text{S21})$$

and calculating the residues leads to the following expression,

$$\int_{c-i\infty}^{c+i\infty} ds_1 \frac{e^{s_1 t_1} e^{-kq_2^2 t_2 \gamma^{-1}} - e^{s_1 |t_1 - t_2|}}{(s_1 + kq_1^2 \gamma^{-1})(s_1 - kq_2^2 \gamma^{-1})} = \frac{2\pi i}{k\gamma^{-1}(q_1^2 + q_2^2)} \left( -e^{-k\gamma^{-1}(q_1^2 t_1 + q_2^2 t_2)} + e^{-kq_1^2 \gamma^{-1} |t_1 - t_2|} \right). \quad (\text{S22})$$

Using this result, we can write  $\langle \tilde{x}(q_1, t_1) \tilde{x}(q_2, t_2) \rangle$  as

$$\langle \tilde{x}(q_1, t_1) \tilde{x}(q_2, t_2) \rangle = \frac{\pi U_a^2 \delta(q_2 + q_1)}{k \gamma^{-1} (q_1^2 + q_2^2)} \left( -e^{-k \gamma^{-1} (q_1^2 t_1 + q_2^2 t_2)} + e^{-k q_1^2 \gamma^{-1} |t_1 - t_2|} \right). \quad (\text{S23})$$

Upon taking the inverse Fourier transform of Eq.(S23) and requiring that  $n_1 = n_2$ , we obtain

$$\langle x(t_1) x(t_2) \rangle = \frac{U_a^2}{4\pi k \gamma^{-1}} \int_{-\infty}^{\infty} dq_2 \frac{1}{2q_2^2} \left( e^{-k q_2^2 \gamma^{-1} |t_1 - t_2|} - e^{-k q_2^2 \gamma^{-1} (t_1 + t_2)} \right) = \frac{\gamma U_a^2}{4\sqrt{k\gamma\pi}} \left( -\sqrt{|t_1 - t_2|} + \sqrt{t_2 + t_1} \right). \quad (\text{S24})$$

Upon evaluating Eq. (S24) at  $t_1 = t_2$ , we obtain our final result for the MSD at long-times, which illustrates the subdiffusive behavior

$$\langle \Delta x(t)^2 \rangle = \langle x(t)x(t) \rangle = \frac{\gamma U_a^2}{4\sqrt{k\gamma\pi}} \sqrt{2t}. \quad (\text{S25})$$

### LOCAL EXPONENT OF MSD FOR SF-ABP SYSTEM

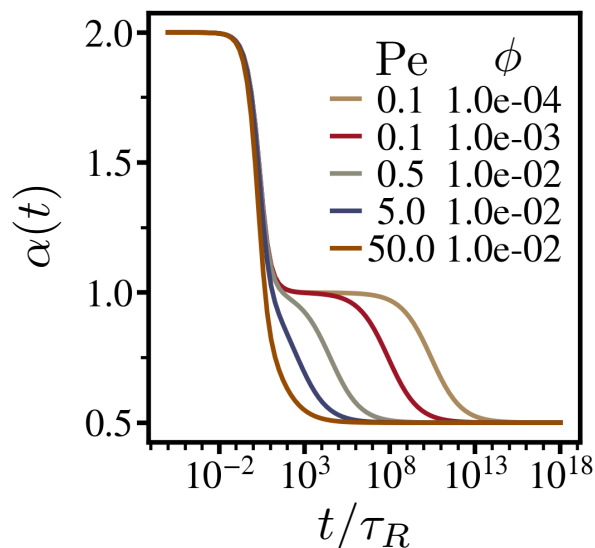


FIG. S3. The local exponent for additional values of  $Pe$  and  $\phi$  using Eq. (27) of the main text. We have selected values that better highlight the diffusive regime at intermediate times. Note that the duration of this regime is highly sensitive to the specific values of  $Pe$  and  $\phi$ . However, it is possible to identify values of  $Pe$  and  $\phi$  that will give a desired profile for the different scaling regimes as well as tune the overall magnitude of the MSD.

\* [sam7808@psu.edu](mailto:sam7808@psu.edu)

- [1] P. M. Centres and S. Bustingorry, Effective edwards-wilkinson equation for single-file diffusion, *Phys. Rev. E Stat. Nonlin. Soft Matter Phys.* **81**, 061101 (2010).
- [2] N. Leibovich and E. Barkai, Everlasting effect of initial conditions on single-file diffusion, *Phys. Rev. E Stat. Nonlin. Soft Matter Phys.* **88**, 032107 (2013).
- [3] M. A. Lomholt and T. Ambjörnsson, Universality and nonuniversality of mobility in heterogeneous single-file systems and rouse chains, *Phys. Rev. E Stat. Nonlin. Soft Matter Phys.* **89**, 032101 (2014).
- [4] B. ten Hagen, S. van Teeffelen, and H. Löwen, Non-gaussian behaviour of a self-propelled particle on a substrate, *arXiv [cond-mat.soft]* (2009).
- [5] M. Graham, *Microhydrodynamics, Brownian Motion, and Complex Fluids*, Cambridge Texts in Applied Mathematics (Cambridge University Press, 2018).